MODELLING OF THIN BACK AMORPHOUS-CRYSTALLINE SI HETEROJUNCTION (BACH) PV

Zahidur R Chowdhury[a], Stefan Zukotynski[a], Nazir P Kherani[a,b,*]
[a] Department of Electrical and Computer Engineering, University of Toronto
10 King's College Road, Toronto, Ontario, Canada M5S 3G4
[b] Department of Material Science and Engineering, University of Toronto
184 College Street, Toronto, Ontario, Canada M5S 3E4
* kherani@ecf.utoronto.ca

ABSTRACT: High efficiency features of heterojunction silicon solar cells and back-contact homojunction solar cells can be integrated in Back Amorphous-Crystalline silicon Heterojunction (BACH) solar cell. Use of only low temperature fabrication processes allows this cell to be fabricated using thin wafers. This article presents a two-dimensional modeling study of the BACH cell concept. A parametric study of the BACH cell has been carried out using Sentaurus after having benchmarked the simulation process. Solar cell efficiency of 24.4% is obtained for AM 1.5 global spectrum with V_{OC} greater than 720 mV and J_{SC} exceeding 40 mA/cm^2, for practical cell parameters. An optical model addressing photo generation accurately in thick and thin absorbers is presented.
Keywords: Back contact, heterojuction, Solar cell, Simulation, BACH, Sentaurus.

1 INTRODUCTION

Fabrication of the recently proposed Back Amorphous-Crystalline Silicon Heterojunction (BACH) solar cell[1] requires only relatively low temperature processing (< 400°*C*). This significantly reduces thermal stress in silicon wafers. Reduced thermal stress enables simplification of the manufacturing process of cells that use very thin wafers, while maintaining the quality of the absorber layer. Solar cell fabrication using very thin crystalline silicon wafers is also an attractive option to reduce material cost while using high quality material.

Further, the BACH cell avoids shadowing losses by relegating electrical contacts to the back surface, which minimizes ohmic losses by maximizing the width of the alternating metal contacts, minimizes surface recombination of carriers through optimum surface passivation and/or configuration of the contacts, and implements favorable light trapping features in order to attain very high conversion efficiency. Therefore, this cell concept integrates high efficiency features of both heterojunction silicon solar cells and back contact homojunction solar cells.

The possibility of achieving a cell efficiency of 24.2%, in mass production, has been demonstrated for the back-contact back-homo-junction cell of SunPower[2]. High-efficiency of 23% using hydrogenated amorphous silicon (aSi:H) - crystalline silicon (cSi) heterojunction with contacts on both sides of the wafer has been reported by Sanyo[3]. The Interdigitated Back Contact Silicon Hetero-Junction (IBC-SHJ) cell [4] and the Back Enhanced Heterostructure with INterDigitated contacts (BEHIND) cell [5] use configurations similar to the BACH cell. Cell efficiencies of 15% and 10.2% have been reported for IBC-SHJ and BEHIND cells, respectively. Simulation studies carried out by Lu *et. al.* [6] and Diouf *et. al.* [7] for the IBC-SHJ cell have been reported using Sentaurus and ATLAS, respectively. In both simulations, the possibility of achieving efficiency greater than 20% was indicated. In their simulations, a thick absorbing layer (~300 μm) and polished front surface with an antireflection coating (ARC) were considered. In order to approximate the performance of a cell with a textured front surface, the front surface was simply assumed to be none reflecting. The Transfer Matrix Method (TMM), utilized in these studies to calculate optical generation, does not completely account for the enhanced optical generation due to multiple reflections of low absorbing light for a textured front surface with an ARC and reflective back surface[8]. This effect is dominant for solar cells fabricated using thin wafers.

This article presents a systematic study wherein Sentaurus is first benchmarked against an analytical study carried out by Tiedje *et al.* [9] vis-à-vis efficiency limit of silicon cells. Then a parametric study of the BACH cell is carried out, showing the dependence of cell performance on various cell parameters including the thickness of the silicon substrate. A description of the model used to evaluate optical generation is also given in this article.

2 DEVICE STRUCTURE

Figure 1 shows the schematic diagram of the simplified BACH cell structure. *n*-type crystalline silicon wafers with 1 Ω·*cm* resistivity and a range of thicknesses are considered for the absorber layer. The substrate is assumed to be passivated with 70 *nm* thick Si_3N_4 layers. The front Si_3N_4 also serves as an anti-reflection coating (ARC). The front surface is assumed to be textured with a Lambertian surface, where incident light is scattered randomly in all directions with equal probability. On the rear-side of the wafer, there are 10 *nm* thick interdigitated strips of *p* and *n* amorphous silicon. Ideal ohmic contacts on *p* and *n* regions are assumed for most part of the study, unless otherwise specified. A 100 μm wide *n*-type aSi region that functions as a back surface field (BSF) and 100 μm gap between *n* and *p* regions are assumed. 100 μm is considered since features with such dimensions can be easily achieved using photolithographic processing. A narrow BSF field is selected to reduce the 'electrical' shading effect as reported by Dross *et al.* [10]. The unit cell is assumed periodic in the lateral direction for the simulations with a period defined by the pitch of the cell.

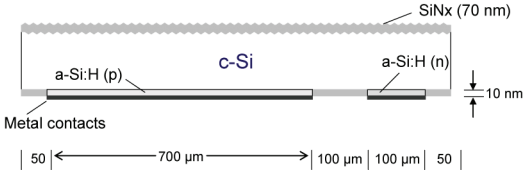

Figure 1: Schematic diagram of the BACH cell.

3 MODELING OF THE BACH CELL

Sentaurus was used to simulate the device physics of the BACH cell by solving Poisson's equation, Electron/Hole Continuity equations and the Drift-Diffusion electron transport relationships. A thermionic emission model was considered for the heterojunction interface. The doping dependent Auger and Shockley-Read-Hall recombination were included or excluded in different cases. The exponential band-tail and Gaussian band-gap trap distributions, and commonly used aSi properties were chosen[11].

3.1 Optical generation

Sentaurus is commercially available semiconductor device simulation software which has recently been used for solar cell simulation [12, 13, 14, 15, 6]. In most of these studies, only thick substrates ($\sim 300\ \mu m$) have been used in the simulations. For such cases, photons with high energy and contributing a significant intensity to the spectrum are absorbed within one pass as they propagate towards the back side of the cell. Further, optical illumination was also considered for a polished front surface with an ARC. In some cases, the reflection at the front surface was simply ignored to estimate the effect of textured front surface. The Transfer matrix model (TMM)[16] was usually used in these simulation studies to calculate transmission and reflection of light in the absorbing media. The use of complex refractive indices to model the absorption of the different layers is allowed in the TMM. Particularly in Sentaurus, TMM is not suitable to accurately represent optical absorption for thick layers and/or for wavelengths with high absorption coefficient, as these lead to numerical overflow conditions. An alternative to the TMM method would be to calculate optical generation by solving Maxwell's equations using the real optical intensity distribution. This method would be the most accurate and Sentaurus does allow its implementation. However, this is a very time-consuming approach. The Beer-Lambert model, which is supported in Sentaurus, does not suffer from the limitations of the TMM model. This model considers a simple exponential decay and does not account for multiple reflections or lateral scattering. The Beer-Lambert model was used in this study to represent the optical spectra on the front and back surfaces due to incident spectrum and reflections.

Performance of solar cells simulated using Sentaurus is benchmarked against an analytical study of cSi solar cell performances carried out by Tiedje *et al.* [9] as a means of verifying our approach to calculating the optical generation. Tiedje *et al.* have shown that the maximum cell efficiency is achieved for wafers of approximately 100 μm thickness owing to the trade-off between short-circuit current, J_{SC} and open-circuit voltage, V_{OC}. Tiedje et al. reported that thicker absorbing layers can result in a higher short-circuit current, J_{SC}. However, because of the increased carrier recombination open-circuit voltage, V_{OC}, decreases. Their study assumed a Lambertian front surface with an ARC for light trapping. The back surface of the cell was considered to be a perfect reflector. Random scattering at the front surface and reflection at the back surface result in multiple reflections of low absorbing light before it reaches the front surface within the escape cone.

The use of the AM 1.5G solar spectrum together with TMM in a Sentaurus simulation is not equivalent to the optical illumination assumed by Tiedje *et al.* Illumination at the front and back surface, with modified intensity and absorption as governed by Beer-Lambert law, can adequately represent the optical generation for the reference case. The spectrum of the incident light at the front and back surfaces are calculated to give absorption similar to the reference case when multiple reflections are considered. Considering absorption enhancement, the absorption probability for such a condition can be expressed [8] as:

$$a(E) = \frac{\alpha(E)}{\alpha(E) + \frac{1}{4[n(E)]^2 t}} \tag{1}$$

where *a(E)* is the absorption probability, α is the absorption coefficient for a particular photon of energy E, $n(E)$ is the refractive index, and t is the thickness of the absorbing layer. In the case of a low absorption coefficient, for example, in the near infrared, the absorption is enhanced almost 40 times as compared to Beer-Lambert law, which applies to the case of an untextured surface:

$$a(E) = 1 - \exp[\alpha(E)t] \tag{2}$$

We can define an effective thickness, $t_{eff}(E)$, such that

$$1 - \exp[\alpha(E) t_{eff}(E)] = \frac{\alpha(E)}{\alpha(E) + \frac{1}{4[n(E)]^2 t}} \tag{3}$$

Solving Equation 3 we get for $t_{eff}(E)$

$$t_{eff}(E) = \frac{1}{\alpha(E)} \ln\left[1 + 4\{n(E)\}^2 \alpha(E) t\right] \tag{4}$$

The number of reflections at the front, $M(E)$, and that at back surface, $N(E)$ for a particular photon energy can be calculated based on the $t_{eff}(E)$ and the wafer thickness, t. Total intensity at the front surface is the sum of incident light intensity and remaining light intensity after being absorbed in one or more round-trips. Equation 5 gives the total intensity at the front surface, $S_f(E)$. Total intensity at the back surface, $S_b(E)$ accounting for multiple reflections, is given in Equation 6.

$$S_f(E) = \sum_{n=0}^{M(E)} s_{fn}(E) S_0(E) e^{-2n\alpha(E)t} \tag{5}$$

$$S_b(E) = \sum_{n=0}^{N(E)} s_{bn}(E) S_0(E) e^{[-(2n-1)\alpha(E)t]} \tag{6}$$

where, $M(E)$ is the number of reflections from the front surface and $N(E)$ is the number of reflections off the back surface, S_0 is the peak intensity for a photon energy defined by the AM1.5G solar spectrum, s_{fn} are the scaling factor for the incident and reflected light intensity at the front surface, and s_{bn} are the scaling factor for the reflected light intensity at the back, needed to account or discard an exponononential element for accurate representation of the optical generation.

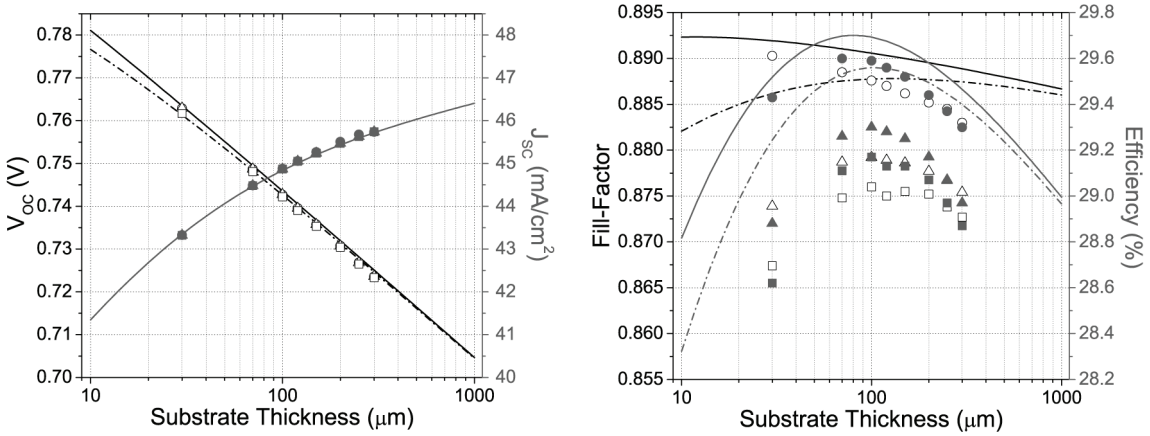

Figure 2: Benchmarking of Sentaurus simulated BACH cell performance against the theoretical formulation of Tiedje *et al.*[9]. Solid and dotted lines represent the theoretical cell performance for J_0 of 0.17 fA/cm^2 and 1 fA/cm^2, respectively. Symbols are used to represent Sentaurus simulated results. Sentaurus results ○/● based on high mobility aSi:H (100× compared to the normal value) without defects in the gap and tails in aSi:H, Δ/▲ based on standard mobility without defects in the gap and tails in aSi:H and □/■ based on standard mobility with defects in the gap and tails in aSi:H. In the graphs, open symbols correspond to the left *y*-axis and the solid symbols correspond to the right *y*-axis.

3.2 Device representation

In the reference article[9], the authors developed an analytical expression to represent the performance of a solar cell considering simply a crystalline silicon layer. The authors also calculated the leakage current for this layer at an ambient temperature by expressing it as an integration of the black-body radiation spectrum and the absorption probability at different photon energies. A simplified expression for the device performance under illumination was derived, as shown in Equation 7, below[9]. The expression is given in terms of leakage current, current loss due to Auger recombination, output voltage and output current, while neglecting the small contribution of free carrier absorption:

$$J_0 \exp\left(\frac{V}{V_t}\right) = e\,t\,c\,n_i^3 \exp\left(\frac{3V}{2V_t}\right) = J_L(1-f) \qquad (7)$$

where, J_0 is the leakage current density, V the output voltage, V_t is the thermal voltage, e is the electron charge, C is the Auger recombination coefficient (where $C = C_n + C_p$), J_L is the short circuit current density or photo generated current density and f is the fraction of current taken out of the layer as an output current.

It should be mentioned that, in Tiedje *et al.*'s study[9] no $p - n$ junction was used to represent the carrier transport of a PV device. The generated electrons and holes were assumed to be collected where they were generated. Moreover, photo generation of carriers in the absorbing layer was assumed to be uniform.

In contrast to Tiedje's model[9], the BACH cell structure with a highly-doped $p - n$ junction is defined in Sentaurus so as to accurately model the carrier transport and collection. Further, a physical optical absorption model was developed and implemented in the present study such that it accurately represents the optical generation which is larger near the front surface due to front surface illumination. Material properties and the physics considered for the simulations were similar to the reference case for the purpose of benchmarking. Other recombination processes, properties of amorphous silicon, especially defect densities, and properties of other layers were gradually incorporated in the study for a progressively more realistic representation of the BACH cell structure.

4 RESULT AND DISCUSSION

4.1 Benchmarking results

Figure 2 shows the comparison between analytical results of the reference case and the results obtained from the Sentaurus simulation of the BACH cells when identical parameters for cSi substrates were considered. The effect of different properties of aSi:H is also demonstrated in Figure 2 obtained using Sentaurus. Cell performances for J_0 of 0.173 fA/cm^2 and 1 fA/cm^2 are also plotted for comparison. J_0 of 0.173 fA/cm^2 corresponds to the calculated dark current based on the black body spectrum while J_0 was ~ 1.0 fA/cm^2 for the simulated BACH cell. Neither surface recombination nor Shockley-Read-Hall (SRH) recombination was considered in these cell simulations. Further, absorption in the top ARC layer was not considered. Open-circuit-voltage and short circuit current of the BACH cell closely match the theoretical results. The deviation in the fill-factor and efficiency depend on the properties of aSi:H. The theoretical values of these parameters for J_0 of 1 fA/cm^2 (dotted lines in the graph) are close to the simulated values when high mobility (100 times that of normal aSi:H material) without defects in the gap and tails in aSi:H were considered for aSi:H. The result deviates from the theoretical result when more practical values of the amorphous material (low mobility and trap densities) are considered.

As shown in Figure 2, short-circuit current, J_{SC}, is observed to increase with increasing substrate thickness while the open circuit voltage, V_{OC}, decreases. Auger recombination is the dominant recombination mechanism for high carrier concentration and this recombination process significantly reduces the open-circuit voltage for the thinner substrates.

4.2 BACH simulation results

BACH cell performance with SRH recombination

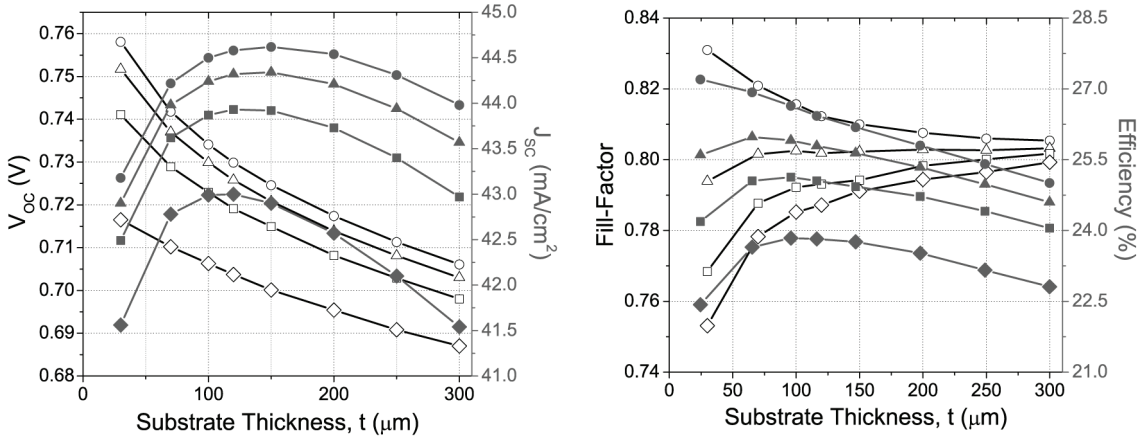

Figure 3: Sentaurus simulation results of BACH cell performance as a function of substrate thickness and passivation quality. ○/● for an SRV (at the cSi and SiN_x interface) of 0 *cm/sec*, Δ/▲ for an SRV of 4 *cm/sec*, □/■ for an SRV of 10 *cm/sec*, and ◊/♦ for an SRV of 25 *cm/sec*, are considered. In the graphs, open symbols correspond to the left *y*-axis and the solid symbols correspond to the right *y*-axis.

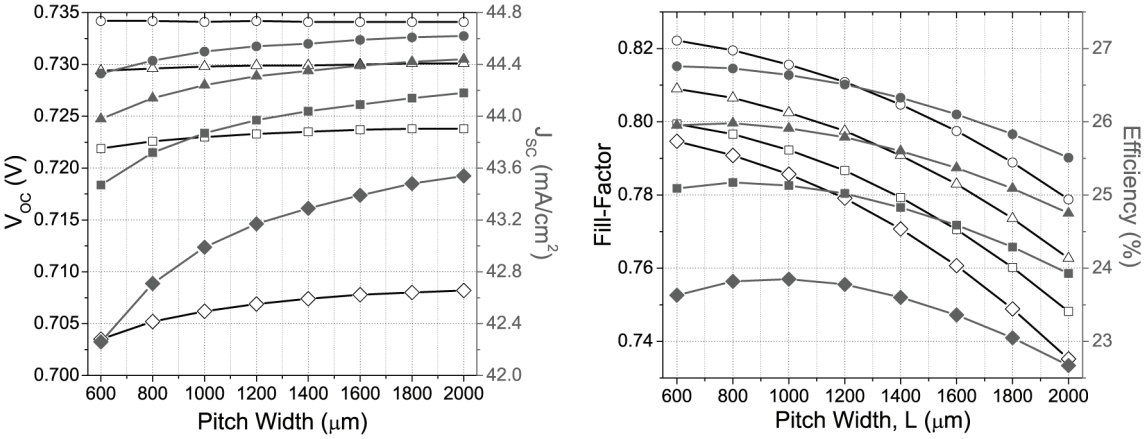

Figure 4: Simulated results of BACH cell performance as a function of pitch width for several surface recombination velocities. ○/● for an SRV (between cSi and SiN_x) of 0 *cm/sec*, Δ/▲ with an SRV (between cSi and SiN_x) of 4 *cm/sec*, □/■ for an SRV (between cSi and SiN_x) of 10 *cm/sec*, and ◊/♦ for an SRV (between cSi and SiN_x) of 25 *cm/sec*, are considered. In the graphs, open symbols correspond to the left *y*-axis and the solid symbols correspond to the right *y*-axis.

and different surface passivation quality was studied. Surface recombination velocity (SRV) measures passivation quality, *i.e.*, the density of interface/surface defects. Figure 3 shows the effect of surface passivation on cell performance. The cell performance deteriorates with poorer passivation (higher SRV values). The performance or efficiency of cells thinner than 50 *μm* or thicker than 150 *μm* are more severely affected by high SRV values. Because of the SRH recombination, the short circuit current, J_{SC}, does not monotonically increase with the substrate thickness. J_{SC} peaks for a substrate thickness of 100 *μm* to 150 *μm* depending on the passivation quality. For the current cell configuration (1 *mm* Pitch, 100 *μm* wide BSF and 100 *μm* wide gap) the thinner substrate performs best for cells with no surface recombination, *i.e.*, an SRV of 0 *cm/s*. The maximum cell efficiency is obtained for thickness around 100 *μm* with excellent SRV of 4 *cm/sec* and moderate SRV ~ 10 *cm/sec*.

Surface passivation giving an SRV of 10 *cm/sec* can be achieved by thermal oxide passivation layers[17] or thin thermal oxide and PECVD grown nitride layers[18]. An SRV of 4 *cm/sec* is reported for intrinsic amorphous silicon (*i*-aSi:H) and PECVD nitride dual layer passivation[19]. The maximum efficiency of 25.9% and 25.1% can be achieved for cells using 100 *μm* thick substrates for an SRV of 4 *cm/sec* and 10 *cm/sec*, respectively. The losses associated with the absorption at the front *i*-aSi:H layer and the resistive transport effects due to the *i*-aSi:H layers, between the absorber and the doped regions, have not been considered in this study.

Cell design was also optimized by varying the pitch of the cell for cells with 100 *μm* substrate thickness. The minimum gap between *p* and *n* doped regions and the minimum width of the BSF region of 100 *μm* are considered. Figure 4 shows the effect of pitch variation for several surface recombination velocities. As shown in the diagram, the optimum value of the pitch is ~1000 *μm*, especially for poorer passivation. Efficiency improves slightly for pitch of less than 1000 *μm*, for better passivated back contact solar cells.

The 'electrical' shading loss becomes dominant for small pitch size owing to the fact that BSF width becomes comparable to the emitter width. The reduced short-circuit current for small pitch width, even without surface recombination, as observed in Figure 4 is due to

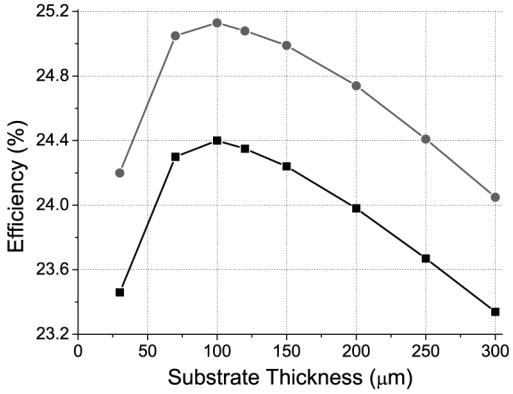

Figure 5: Effect of metal work-function and substrate thickness. Cell performance for • ohmic contact and ■ nickel on the anode while using aluminum on the cathode with an SRV of 10 *cm/sec* and other recombination processes.

the fact that minority carriers (holes) recombine at the BSF before being collected at the emitter. Cell performance for large pitch width (greater than 1000 μm) is low because of the low fill-factor. Diffusion lengths of carriers, that depend on mobility and lifetime of carriers, governs the performance of cells with such configuration.

Finally, the variation in the work-functions of the metal electrodes was introduced to obtain a more representative result of the performance of the BACH cell. Nickel was used as the anode and aluminum was used as the cathode for contacts close to being ohmic. Figure 5 shows the variation of efficiency as a function of substrate thickness with a 1000 μm pitch. An SRV of 10 *cm/sec* and other recombination processes are also considered. The maximum efficiency of 24.4% is obtained for a 100 μm thick substrates with J_{SC} = 43.9 mA/cm^2, FF = 77.04% and V_{OC} = 0.722 V.

5 CONCLUSION

BACH cell simulation results are presented in this article. A Lambertian front surface and reflective back surface is considered for the light trapping. Optical intensity is calculated at the two surfaces to ensure proper optical generation using Beer-Lambert's law for optical absorption. Cell performance for different absorber layer thickness, passivation parameter, and electrode spacing, are considered. The maximum efficiency is 24.4% for the simulated cell structure for 100 μm thick cSi absorbing layer with passivation layers having 10 *cm/sec* SRV. Radiative, Auger and SRH recombination are also considered. The optimum cell configuration has 100 μm wide gap between emitter and BSF. The width of the BSF and emitter is 100 μm and 700 μm, respectively. This study shows the prospects of the BACH cell using thin cSi substrates.

ACKNOWLEDGMENT

This work was supported through grants from Natural Sciences and Engineering Research Council of Canada, Ontario Centers of Excellence, and the Ontario Research Fund − Research Excellence program, in collaboration with Arise Technologies Corporation.

REFERENCE

[1] A. Hertanto, H. Liu, D. Yeghikyan, B. G. Rayaprol, N. P. Kherani, S. Zukotynski, IEEE 34th PVSC (2009).

[2] P. J. Cousins, D. D. Smith, H. C. Luan, J. Manning, T. D. Dennis, A. Waldhauer, K. E. Wilson, G. Harley, W. P. Mulligan, Proceedings of the 35th IEEE Photovoltaic Specialists Conference (2010 In Press).

[3] M. Taguchi, Y. Tsunomura, H. Inoue, S. Taira, T. Nakashima, T. Baba, H. Sakata, E. Maruyama, Proceedings of the 24th European Photovoltaic Solar Energy Conference (2009) 1690.

[4] B. Shu, U. Das, J. Appel, B. McCandless, S. Hegedus, B. R., 35th IEEE Photovoltaic Specialists Conference (PVSC) (2010) 3223.

[5] M. Tucci, L. Serenelli, E. Salza, M. Ratte, S. De Iuliis, L. Geerligs, D. Caputo, A. Nascetti, G. de Cesare, Thin Solid Films 516 (2008) 6771.

[6] M. Lu, U. Das, S. Bowden, S. Hegedus, R. Birkmire, Progress in Photovoltaics: Research and Application (2010).

[7] D. Diouf, J. Kleider, T. Desrues, P.-J. Ribeyron, Materials Science and Engineering B 159-160 (2009) 291.

[8] E. Yablonovitch, Journal of Optical Society of America 72 (7) (1982) 899.

[9] T. Tiedje, E. Yablonovitch, G. D. Cody, B. G. Brooks, IEEE Transaction on Electron Devices 31(5) (1984) 711.

[10] F. Dross, E. VanKerschaver, G. Beaucarne, Proceedings of the 15th International Photovoltaic Science and Engineering Conference, Shanghai, China (2005).

[11] R. E. I. Schropp, M. Zeeman, Kluwer Academic, Dordrecht, 1998.

[12] O. Nichiporuk, A. Kaminski, M. Lemiti, A. Fave, V. Skryshevsky, Solar Energy Materials and Solar Cells 86 (2005) 517.

[13] M. Lu, S. Bowden, R. Birkmire, Conference on Numerical Simulation of Optical Device, Newar (2007) 55.

[14] M. Hermle, Universit¨at Konstanz, Dissertation thesis (2008).

[15] J. Renshaw, M. H. Kang, V. Meemongkolkiat, A. Rohatgi, D. Carlson, M. Bennett, Conference Proceedings of the 34th IEEEPVSC (2009).

[16] M. Born, E. Wolf, Pergamon Press, Oxford, 1964.

[17] B. Hoex, J. Schmidt, P. Pohl, M. C. M. van de Sanden, W. M. M. Kessels, Journal of Applied Physics 104 (2008) 044903.

[18] Y. Larionova, V. Mertens, N.-P. Harder, R. Brendel, Applied Physics Letters 96 (2010) 032105.

[19] D. S. Stepanov, Z. R. Chowdhury, N. P. Kherani, in: Photonics North, Ottawa, Canada.